American Mineralogist, Volume 91, pages 1688–1698, 2006

Deep metastable eutectic condensation in Al-Fe-SiO-H_2-O_2 vapors: Implications for natural Fe-aluminosilicates

Frans J.M. Rietmeijer,[1,*] Joseph A. Nuth,[2] Pierre Rochette,[3] Jannie Marfaing,[4] Aurora Pun,[1] and James M. Karner[1]

[1]Department of Earth and Planetary Sciences, MSC03-2040, 1-University of New Mexico, Albuquerque, New Mexico, 87131-0001, U.S.A.
[2]Laboratory for Extraterrestrial Physics, Code 691, NASA Goddard Space Flight Center, Greenbelt, Maryland, 20771, U.S.A.
[3]CEREGE, CNRS-Université d'Aix-Marseille 3, BP80, Europole de l'Arbois, 13545 Aix en Provençe Cedex 4, France
[4]L2MP, CNRS-Université d'Aix-Marseille 3 Faculté des Sciences de Saint Jérôme, Case 142, 13397 Marseille Cedex 20, France

Abstract

Vapors of Al-Fe-SiO-O_2-H_2 having two different compositions produced ferroaluminosilica grains as a function of agglomeration and fusion along mixing lines in the Al_2O_3-FeO-SiO_2 system that are defined by the predictable, deep metastable eutectic (DME) compositions of the smallest condensate grains. Disorder of these amorphous grains is higher than in quenched glass of identical composition, which is the very property of dissipative structures (Prigogine 1978, 1979) that are states of organization of matter where disequilibrium becomes a source of order. Iron-oxidation states control ferrosilica condensate compositions. We present the first magnetic measurements showing a high Fe^{3+} content in condensed ferrosilica grains. The Fe-cordierite grain composition is primarily the result of predictable non-equilibrium condensation, not the bulk gas phase composition. Natural terrestrial and anthropogenic (e.g., smelters, coal fly ash) Fe-cordierite might well be a metastable phase due to kinetically controlled processes. Amorphous Mg,Fe-bearing aluminosilica dust in chondritic interplanetary dust aggregates and (rare) Mg,Fe-aluminosilicates in meteorites might have condensed via similar processes.

Keywords: Vapor phase condensation, ferroaluminosilica vapor, non-equilibrium condensation, deep metastable eutectics, magnetic measurements, Fe-cordierite

Introduction

Planetary materials, as described in the *Reviews in Mineralogy* volume edited by J.J. Papike (1998), are fundamentally the result of dust aggregation. An axiom of cosmochemistry holds that dust or its precursor was initially condensed from an O-rich, Si-bearing vapor. Once formed, the condensed solids could then be processed in molecular clouds and circumstellar disks such as in the solar nebula 4.56 billion years ago. Understanding the condensation process is critical to appreciate the properties of the nanometer-sized condensed solids that ultimately define the chemical compositions and minerals in comets, asteroids, and the terrestrial planets. The similarity between the solar photosphere and the chemically primitive CI carbonaceous chondrite meteorite compositions is considered as evidence that the solar nebula gas had a bulk chondritic (or CI) composition (Anders and Grevesse 1989). At one time during its evolution, the solar nebula contained condensed solar nebula dust and surviving dust from the molecular cloud fragment wherein the nebula had formed. The latter, pre-solar, dust included silicates (Messenger 2000; Keller et al. 2000) that had formed around other, older stars by vapor-phase condensation. It is important that the common silicates [e.g., forsterite, diopside (Rietmeijer 1999)], Mg-rich ferromagnesiosilica grains (Rietmeijer et al. 1999a), GEMS (glass with embedded metals and sulfides; Bradley 1994; Bradley et al. 1999), and Fe,Ni-sulfides in chondritic aggregate, interplanetary dust particles (IDPs) collected in the Earth's lower stratosphere (for reviews see, Rietmeijer 1998, 2002), are also present around O-rich stars in different stages of stellar evolution (Bouwman et al. 2001; Molster and Waters 2003) and "pure" Mg-silicate crystals are observed in stellar outflows (Nuth et al. 2002).

Mostly based on theoretical considerations, condensation of a solar nebula gas has been considered to be an equilibrium process that would yield an orderly sequence of stoichiometric minerals ranging from refractory (Ca,Ti,Al-rich) high-temperature minerals to low-temperature silicates (Larimer 1967, 1988; Grossman and Larimer 1974, Wood and Hashimoto 1993; Petaev and Wood 1998, among many others). Kinetic factors almost certainly are involved in this process and yet the notion of equilibrium condensation has been remarkably persistent, including variations that considered sub-nebular domains with non-chondritic gas compositions. It also has been pointed out that a condensing vapor would not contain stoichiometric gas molecules (Donn and Nuth 1985), such as Mg_2SiO_4, to form equilibrium forsterite (Lord 1965). Perhaps more devastating to equilibrium condensation models is the fact that despite long searches in meteorites (Wark 1979), there is no evidence for sequential condensation of the predicted stoichiometric equilibrium minerals. It is timely then to explore a stellar kinetic (condensation) model of simple metal oxides and non-stoichiometric solids such as Mg-SiO_x, Fe-SiO_x, and Al-SiO_x (Nuth et al. 2000) as an alternative process.

Deep metastable eutectic (DME) condensation

Prigogine (1978, 1979) showed that conditions of nonequilibrium could establish states of organization of matter where disequilibrium becomes a source of order referred to as dis-

* E-mail: fransjmr@unm.edu

0003-004X/06/0010–1688$05.00/DOI: 10.2138/am.2006.2102

sipative structures. De (1979) introduced this concept to vapor condensation in astronomical environments when a cooling vapor experiences excursions in condensation and evaporation rates prior to reaching the equilibrium state when the grain and gas temperatures are equal (Fig. 1). When pre-equilibrium condensates are preserved, they will be dissipative structures with extreme disorder, that is, these solids are more disordered than quenched glass of identical composition. Highmore and Greer (1989) and Aasland and McMillan (1994) postulated that a dissipative structure arising from an entropy catastrophe could explain the DME phase relationships observed in some metal-oxides and amorphous alloys.

In vapor-condensation experiments, a "hot" vapor is quenched to a "low" temperature, whereby "hot" and "low" are relative designations. In our experiments, pre-mixed Al-SiO-H_2-O_2 (Rietmeijer and Karner 1999), Fe-SiO-H_2-O_2 (Rietmeijer et al. 1999b), Mg-SiO-H_2-O_2 (Rietmeijer et al. 2002a), and Mg-Fe-SiO-H_2-O_2 (Rietmeijer et al. 1999a) vapors were quenched to a temperature well below the solidus and glass transition temperatures. The invariably amorphous condensed dust has distinct compositions that do not match stoichiometric silicate minerals. Some of the condensed, mixed, aluminosilica, magnesiosilica, and ferrosilica grains have: (1) a serpentine dehydroxylate composition (e.g., $Mg_3Si_2O_7$) (MacKenzie and Meinhold 1994); and following the same terminology, (2) a talc dehydroxylate composition[1] (e.g., $Mg_6Si_8O_{22}$); or (3) a low-silica (~5 wt% SiO_2) ferro- or magnesio-silica composition (Fig. 2). Predictable DME compositions co-occur, but with relative abundances that are sensitive to the bulk metal-oxide/silica ratio of the condensing vapor, and they are a result of rapid vapor quenching (Rietmeijer et al. 2004).

These results show that non-equilibrium vapor phase condensation yields highly disordered, amorphous condensates with a predictable composition in binary systems that have at least two eutectic points. Condensation in an Mg-Fe-SiO-H_2-O_2 vapor mimics DME dust formation in the binary MgO-SiO-H_2-O_2 and FeO/Fe_2O_3-SiO-H_2-O_2 vapors and the resultant smoke is a random mixture of amorphous ferrosilica and magnesiosilica

[1]The common layer silicate found in the matrix of undifferentiated meteorites, except the CI carbonaceous chondrites, and in chondritic aggregate IDPs, occurs as tiny purely Mg,Si [O] protocrystallites of no district morphology characterized by smectitic lattice fringes (see Papike 1998). Identical protophyllosilicates were produced in a hydrated condensed magnesiosilica smoke in amorphous material of $Mg_6Si_8O_{22}$ composition, which prompted a smectite dehydroxylate designation (Rietmeijer et al. 2004). Strictly speaking this amorphous material is talc dehydroxylate, which will be used in this paper.

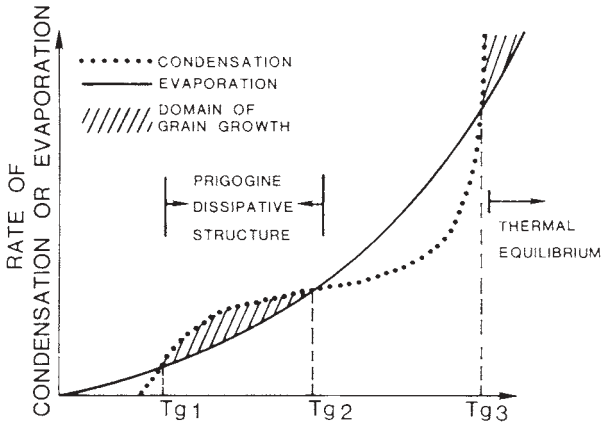

FIGURE 1. Condensation or evaporation rates as a function of grain temperature (Tg), in a non-equilibrium state prior to thermal equilibrium. The schematic diagram shows the conditions to develop a dissipative structure as defined by Prigogine (1978, 1979) (see text). Reprinted from De (1979) with kind permission of Springer Science and Business Media and the author.

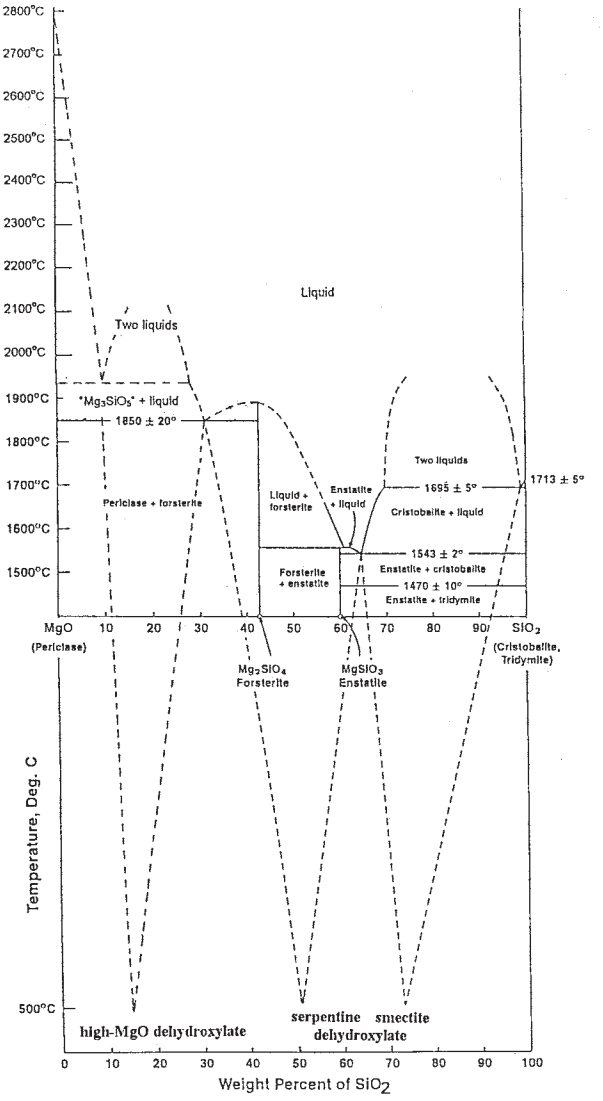

FIGURE 2. The MgO-SiO_2 phase diagram (see Ehlers 1972) modified to accommodate three DME compositions observed in condensed magnesiosilica smokes (Rietmeijer et al. 2002a). The modification involves a eutectic in the silica-poor portion of the diagram. NOTE: the positions of the metastable eutectics are only based on measured condensate compositions and the nominal quench temperature (500 °C) in the experiment. There is no implication that DMEs have a fixed temperature in a phase diagram. This figure is reprinted from Rietmeijer and Nuth (2005), Copyright 2005, with permission from Elsevier.

domains (Rietmeijer et al. 1999a). There are no ferromagnesiosilica condensates because complete solid solution in the FeO-MgO and Fe_2SiO_4-Mg_2SiO_4 systems prevents DME dust formation. We have postulated that ternary ferromagnesiosilica dust can only be formed via agglomeration and fusion along mixing lines defined by DME magnesiosilica and ferrosilica condensate compositions during condensation and auto-annealing (see below). Consequently, the distribution of ferrosilica and magnesiosilica DME condensate compositions predicts unique Mg-rich ferromagnesiosilica compositions as a result of grain fusion along the mixing lines. That such agglomeration and fusion of DME magnesiosilica and ferrosilica dust has occurred in extraterrestrial environments is supported by the Si-rich talc dehydroxylate compositions of sub-micrometer Mg-rich ferromagnesiosilica spherical units in chondritic aggregate IDPs (Rietmeijer 1998, 2002). This observation is not proof for a stellar kinetic (condensation) model (Nuth et al. 2000) but we submit that non-equilibrium vapor condensation can yield testable predictions about the compositions of dust during solar nebula condensation.

AUTO-ANNEALING

Refractory molecules agglomerate and at some point they form the smallest recognizable grains observed by transmission electron microscope (TEM) analyses of condensed smokes. We have no information on condensate compositions at the molecular level. Thus, DME condensation will be defined by the crystallographic and chemical properties of the smallest individual condensate grains that we can observe in our samples, typically 2 to 10 nm in diameter. Grains in a highly porous smoke of interconnected necklaces may typically reach up to ~100 nm in size. There is a marked discontinuity in the size distribution at about 20–30 nm due to condensed grain growth by fusion (Rietmeijer and Nuth 1991; Rietmeijer and Karner 1999; Rietmeijer et al. 1999b).

Condensation takes place inside the closed experimental container wherein smokes are collected on substrates placed inside the apparatus. The samples are mixtures of porous smoke and dense smoke clusters that could be either a condensation feature or one superimposed on condensates when "cold" condensates already deposited on the collectors are hit by "hot" settling condensates. Crystallization of condensed stoichiometric oxides to tridymite, periclase, and Fe-oxides provides latent heat to the condensing system. Condensate heat dissipation is an inherent part of the experiment that will affect the condensates. Auto-annealing is the process that refers to all chemical, textural, and crystallographic modification that occurs as part of the condensation experiment itself (Rietmeijer and Nuth 1991; Rietmeijer et al. 2002b). Auto-annealing can lead to larger grains, often with an irregular surface of either (partially) fused smaller grains or smooth grains with compositions that can be intermediate between the DME compositions. The latter did not happen in the condensing Mg-Fe-SiO-H_2-O_2 vapor (Rietmeijer et al. 1999a), but was observed in two smokes condensed in Al-Fe-SiO-O_2-H_2 vapors; the latter will be the topic of this paper. For Fe-containing condensates, there is another variable affecting grain composition because oxygen fugacity during vapor condensation and auto-annealing cannot be buffered due to the dynamic nature of the reactions. Lack of buffering results in variable Fe^{3+}/Fe^{2+} ratios of condensed grains. In fact, in the FeO-Fe_2O_3-SiO_2 system, the ferrosilica talc dehydroxylate condensates had two different DME compositions linked to variable Fe^{2+}/Fe^{3+} ratios (Rietmeijer et al. 1999b).

We predict extensive ternary chemical mixing in the Al_2O_3-FeO-SiO_2 system because the topology of all three constituent binary phase diagrams allows for condensates with a DME composition to form. Based on previous observations of ferrosilica condensates (Rietmeijer et al. 1999b), a variable Fe^{2+}/Fe^{3+} ratio will affect Fe-containing grain compositions. The experiments were selected because, in another case of serendipity in science, the post-condensation thermal dampening of the system was discontinuous over a period of several minutes. Fusion and homogenization along predictable mixing lines that are defined by the smallest DME condensate grains has produced larger grains with uniform chemical compositions independent of the bulk gas phase composition. In this paper, we report the first magnetic measurements on a ferrosilica smoke and on the sizes and compositions of grains that condensed in two different Al-Fe-SiO-H_2-O_2 vapors wherein they could evolve during auto-annealing as part of the experiment.

EXPERIMENTAL PROCEDURES

Condensation experiments

Vapors of variable SiO_x, AlO_x, and FeO_x mixtures were condensed at different temperatures between 25 to 775 °C and total pressures of ~100 torr, to study the infrared (IR) properties as a function of bulk composition, post-condensation thermal annealing, and hydration (Nuth et al. 1988, 2000, 2002). For this study, we selected two smokes with very different bulk compositions, S525 and S25, which were produced in the experimental apparatus as described in Nelson et al. (1989). In the case of S525, tri-methyl aluminum, pentacarbonyl iron, and silane, all significantly diluted in hydrogen gas, passed through a resistively heated alumina furnace at 525 °C together with a separate stream of oxygen gas. The reaction product, a fine-grained smoke, was collected downstream from the furnace on a copper surface at room temperature for later analyses. The general apparatus can be thought of as simply a slightly modified Bunsen burner operating within a vacuum system that allows us to control the total pressure of the system. In the case of S25, the furnace heater broke just before we had established a steady flow of reactive gases. Because the system appeared to continue to make "smoke" even as it cooled rapidly toward room temperature, we allowed the failed experiment to continue, curious as to what might form under such low-temperature conditions. Although the gas did cool to just above room temperature and oscillated between ~30 to ~55 °C in a series of periodic explosions for about an hour, a steady state was never really established. Sample S25 represents a mixture of the smokes made throughout the experiment, from the first few minutes at temperatures above 500 °C through the cooling period (~10 min), and through the steady oscillations in temperature and periodic explosions (about every 3 to 5 min at the high-temperature limit) that we allowed to continue for about an hour. To say that sample S25 represents an extremely unequilibrated composition is definitely understating the range in formation conditions represented in this smoke.

Analytical and transmission electron microscope analyses

Serial ultrathin (~90 nm) sections were prepared from a small portion of each sample. Sections were placed on a holey carbon thin-film supported by a standard 200 mesh Cu grid for study in a JEOL 2000FX analytical and transmission electron microscope (ATEM, at UNM) operated at an accelerating voltage of 200 keV. The TEM was equipped with a Tracor-Northern TN-5500 energy-dispersive spectrometer (EDS) for in situ quantitative chemical analysis with a relative error <10% using a probe size of ~10 nm in diameter that in most cases is similar to the grain size or smaller. Artifacts in grain composition could arise from overlapping grains smaller than the section thickness. Prior to analysis, each grain was viewed using a "through-focus" technique to check for additional grains along the electron beam path; the location of each EDS analysis was also recorded on

TEM photomicrographs to allow a check of the original images for any spurious artifacts. We report only high-fidelity analyses. Imaging in the TEM viewing mode is at a 0.2 nm spatial resolution. Grain sizes were measured directly from calibrated TEM images with a 10% relative error. TEM imaging and selected area electron diffraction (SAED) confirmed the amorphous nature of the condensed grains. The statistical analyses include a normalcy test for the distributions using the ratio of the data range and standard deviation (1σ) as a function of population size at a chosen 95% level of confidence. A two-tailed t-test, at the 10% significance level for the equality of population means, was used to reject (or accept) the null-hypothesis that two population means cannot be from identical populations.

Magnetic characterization of iron oxidation states in a FeSiO smoke

For magnetic measurements, a 1.41 mg sample was pressed in a Perspex container and its magnetization vs. magnetic field was measured using a Micromag vibrating sample magnetometer (CEREGE, CNRS). For details on this technique, we refer the reader to Dunlop and Özdemir (1997). The very low observed signal necessitated careful averaging and holder subtraction. Variable temperature measurements were inconclusive due to higher noise levels compared to room-temperature measurements. Mass was measured using a μg-precision balance. Mass-normalized parameters were computed per kilogram of Fe_2O_3 based on a bulk composition of 32.5% FeO reported by Rietmeijer et al. (1999b), or 36.1% as Fe_2O_3.

In addition, we used a Bruker EMX 10/12 Electron Spin Resonance (ESR) spectrometer (CEREGE, CNRS) operating at $\nu_0 = 9.396$ GHz ($\gamma = 2$ corresponds to 335 mT) at room temperature. This non-destructive technique is widely used for powders containing paramagnetic ions, even in low concentration. The ESR signal detects the interaction between the electronic spins submitted to the influence of both local and external magnetic fields. The associated parameters of the signal, mainly the Landé factor (g) or position and width of the resonance lines, are indicative of the ion type and its oxidation state.

Observations

The bulk compositions of the smokes selected for ATEM analyses, viz. S25 (condensed at 25 °C) and S525 (condensed at 525 °C), are a proxy of the vapor phase compositions (Table 1). Smoke S25 shows necklaces of condensed grains with the variable degrees of neck formation and fusion typical for fluffy vapor-condensed smokes (Fig. 3). Condensation favored formation of domains of pure silica and mixed aluminosilica and ferrosilica grains that are randomly mixed in the deposited smoke (Nuth et al. 2000). The pure silica smoke is coarser-grained than the mixed smokes whereas grain sizes in the ferroaluminosilica domains (Fig. 3) are larger than in the binary smoke domains. Smoke S525 shows a similar gross domain texture, but the proportion of fluffy smoke to coarse-grained domains is significantly lower than in S25; also, the necklaces in S525 are much shorter (Fig. 4). Smoke S525 shows ample evidence for extreme grain growth during dust condensation, expressed by the high number density of large spheres (Fig. 4) in many parts of this sample. Large spheres occur isolated and arranged in short necklaces, often with considerably advanced neck formation (Fig. 5). There

TABLE 1. Bulk compositions of experimentally condensed ferroaluminosilica smokes obtained by electron microprobe analyses (EMPA; Nuth et al. 1988) and analytical transmission electron microscope analyses ATEM (this work; mean = ±1σ standard deviation)

Sample	Bulk Composition					
	EMPA			ATEM		
	SiO_2	Al_2O_3	FeO	SiO_2	Al_2O_3	FeO
S525	69.8	22.6	7.6	63.9 ± 12.2	29.1 ± 9.0	7.0 ± 5.2
S25	85.5	11.5	3.0	79.7 ± 21.7	16.4 ± 22.4	3.9 ± 3.6

Notes: The lower silica content obtained by ATEM, albeit within the standard deviation, is an analytical bias due to avoidance of pure silica domains in the smokes. For comparison, the chondritic (CI) composition based on the Orgeuil meteorite is $SiO_2 = 54$, $Al_2O_3 = 3$, and FeO = 43 wt%.

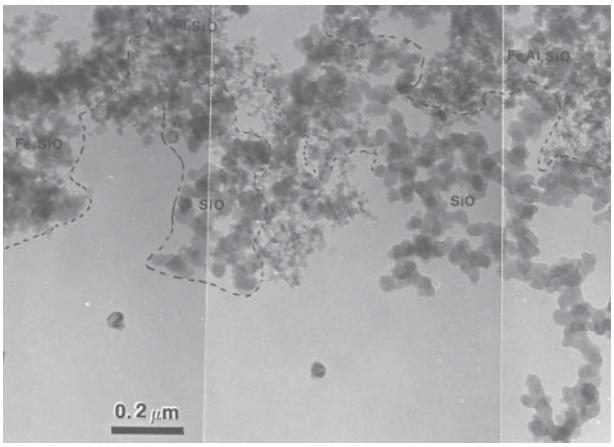

FIGURE 3. A TEM composite image of an ultrathin section of ferroaluminosilica smoke S25 consisting of pure silica, binary ferrosilica, and aluminosilica, and ternary ferroaluminosilica domains delineated by dotted lines (modified after Nuth et al. 2000). The light-gray background in this and other images in this paper is caused by the embedding epoxy. The scale bar is 0.2 μm.

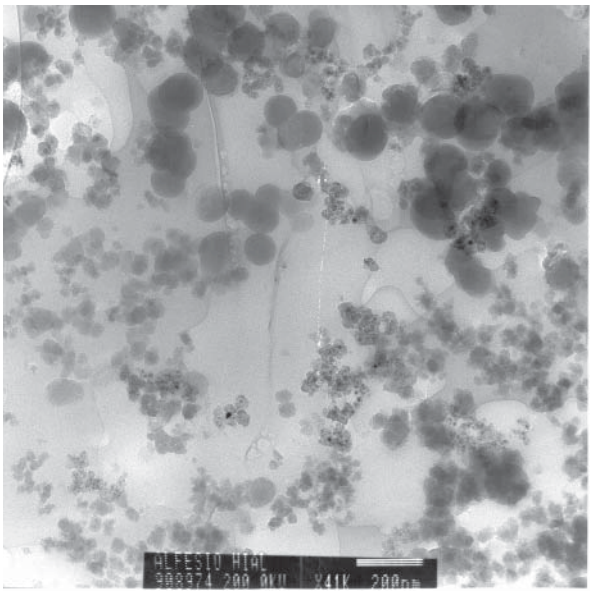

FIGURE 4. TEM image of an ultrathin section of smoke S525 showing its typical fine-grained necklaces and abundant smooth spheres after complete fusion and homogenization of agglomerated grains an small spheres zed condensate grains. The textured background in this and other TEM images is the holey-carbon thin film that supports an ultrathin slice of epoxy-embedded sample. The scale bar is 200 nm.

is no evidence that any of the condensed grains in either sample has an ordered, crystalline structure.

Grain compositions and size distributions

The grain compositions and size distributions in Table 2 are arranged in two columns for: (1) smoke grains, meaning extremely rare isolated grains, grains in necklaces, and in massive (low-porosity) clusters; and (2) spheres due to fusion and homogenization of aggregates of DME condensate grains and the continuing fusion and homogenization of smaller ferroaluminosilica spheres. The observation that grains and spheres with identical composition are common also suggests a genetic relationship of agglomeration and complete fusion in the necklaces and grain clusters. The distributions of grain compositions in S525 and S25 are broadly similar, but whereas ferroaluminosilica grains and spheres abound in S525, they are rare in S25 (Fig. 6). S525 (Fig. 6a) contains no high-Al aluminosilica grains, but S25 does (Fig. 6b).

More than 90% of the grains are spherical; the remainders are slightly sub-spherical and these grains tend to be limited to the upper range of the size population. Each size population, identified by its mean and standard deviation (Table 2), has a log-normal distribution indicating size sorting controlled by grain-grain collisions followed by neck formation and fusion into larger grains. Diagrams of f/f_{max} vs. r/r_{mean} (f = frequency; r = grain radius) (Baronnet 1984) of the grain sizes in these populations shows that this Ostwald ripening process follows second-order growth kinetics, i.e., it is not primarily defined by volume diffusion. For the smallest pure silica, ferrosilica [FeO: 12.7 wt% (S525); 14.5 wt% (S25)], and low-FeO ferroaluminosilica grains in both samples, the f/f_{max} vs. r/r_{mean} relationship supports a juvenile distribution with the preservation of the smallest condensate grains. The same conclusion can be reached for high-FeO ferroaluminosilica grains in S525. The smallest aluminosilica grains (Al_2O_3 = 15 and 47.1 wt%) in both smokes show a similar but evolved distribution wherein the smallest grains have disappeared completely via ripening.

The grain compositions in Table 2 are arranged, from top to bottom, from pure silica, ferrosilica, aluminosilica, and ferroaluminosilica to pure alumina. The size distributions

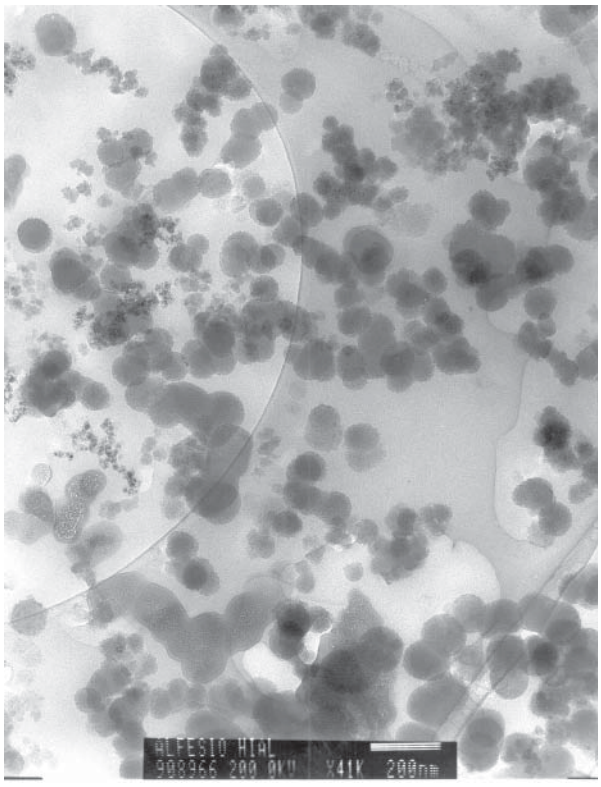

FIGURE 5. TEM image of an ultrathin section of smoke S525 showing a high concentration of single spheres and spheres arranged in short necklaces with variable degrees of fusion. The fine-grained necklaces (black; on the left) consist of ferroaluminosilica grains. The scale bar is 200 nm.

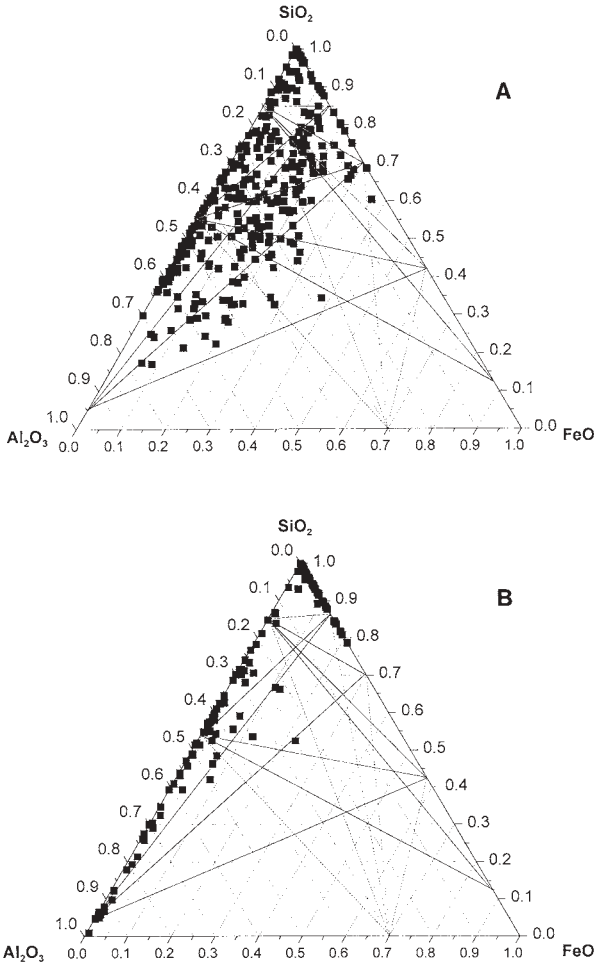

FIGURE 6. Ternary SiO_2-Al_2O_3-FeO diagrams with the grain compositions in S525 (**a**) and S25 (**b**). The abundant pure silica grains in each sample are not indicated. The solid lines across the diagrams are mixing lines between the smallest condensates with deep, metastable aluminosilica and ferrosilica eutectic compositions. The dashed lines connect observed DME compositions to a potential DME composition on the Al_2O_3-FeO join (see discussion). Iron is presented as Fe^{2+}, but we recognize variable Fe^{2+}/Fe^{3+} ratios as identified by magnetic measurements of a ferrosilica smoke.

TABLE 2. Grain compositions (wt%) and sizes (nm) of pure silica, ferrosilica, aluminosilica, and aluminoferrosilica in smoke samples S25 and S525

Composition			Smoke grains (nm)			Spheres (nm)			
SiO_2	Al_2O_3	FeO	Range	$\mu \pm \sigma$	50%	Range	$\mu \pm \sigma$	50%	Sample
100			2–39	11.8 ± 7.2	8.9	37–115	75		S525
100			6–29	16.2 ± 6.2	12.2	21–60	35.9 ± 8.7	32.9	S25
100						57–175	91.4 ± 37.9	77.6	S25
97.7		2.3	2–15	8.9 ± 3.8	7.1				S525
96.6		3.4				12–115	37.8 ± 29.8	22.6	S525
87.3 ± 4.2		12.7 ± 4.2	2–20	7.3 ± 4.2	5.4				S525
87.3 ± 4.2		12.7± 4.2	35–60	45					S525
85.5 ± 4.1		14.5 ± 4.1	2–13	4.2 ± 2.3	3.3	5–56	21.2 ± 10.1	17.2	S25
69.0		31.0		5*					S525
79.0		21.0				24–90	55		S525
86.0	14.0			12*		37–220	98.3 ± 41.3	90.4	S525
85.0	15.0			12*					S25
52.9± 10.5	47.1 ± 10.2†		4–10	7.9 ± 2	3.7				S525
52.9± 10.5	47.1 ± 10.2†		10–50	22.8 ± 8.8	19.8				S525
52.9 ± 14.6	47.1 ± 14.5†		17–53	35.2 ± 11.5	30.5	135–200	175		S25
58.2 ± 15.1	41.8 ± 11.1					37–220	98.3 ± 41.3	90.4	S525
86.6 ± 4.6	6.3 ± 2.2	7.1 ± 3.8	2–46	11.6 ± 10.2	5.8				S525
90.1 ± 3.3	6.9 ± 3.7	3.0 ± 1.7				36–210	93.9 ± 39.2	78.8	S525
56.9 ± 15.1	25.8 ± 14.9	17.3 ± 6.7	2–17	6.0 ± 3.1	3.7				S525
56.9 ± 15.1	25.8 ± 14.9	17.3 ± 6.7	15–55	30.9 ± 11.6		50–73	59.1 ± 8.9		S525
47.4 ± 3.1	30.2 ± 3.5	22.4 ± 3.1				170–340	220.0 ± 49.6		S525
53.0	25.0	22.0					450*		S25
6.1 ± 1.1	93.9 ± 1.3					140–225	180		S25
	100						155*		S25

Notes: The population mean (μ) ± standard deviation (σ) is only given when the population size is >10; the populations consist overwhelmingly of >50 measurements with many having >100 measurements. Otherwise only average values are provided. The column "50%" indicates that half of the population of grains or spheres is smaller than the value listed. The upper limit matches the mullite composition (Al_2O_3 = 72 wt%). Rare condensate grains have a stoichiometric silicate composition and can be crystalline, e.g., forsterite (Rietmeijer et al. 2002b, 2004).

* Only one grain.

† These grains contain ranges 22 to 71 wt% Al_2O_3.

for each composition are listed for smoke grains and spheres (when appropriate) that indicate a genetic relationship between grains and spheres. Multiple size populations for a given grain or sphere composition indicate isochemical coarsening due to grain growth. To explore condensate grain-size differences in the samples, a double-tailed t-test was applied. The t-test of the equality of means for pure silica smoke grains in S25 and S525 finds that the null-hypothesis cannot be rejected, i.e. there is no evidence to suggest that the two size groups came from populations having different means. A similar conclusion was reached for the smallest ferrosilica grains (FeO = means of 12.7 and 14.5 wt%). Whereas the smallest aluminosilica grains were preserved in S525, these grains did not survive in S25 wherein these smoke grains match those of the evolved population in S525. This behavior may be explained by local variations in three-dimensional grain stacking within the smoke. Ferroaluminosilica grains in S525 (SiO_2 = 56.9; Al_2O_3 = 25.8; FeO = 17.3 wt%; Table 2) show a similar feature. The smallest grains (6 nm) form short, scattered necklaces whereas larger grains (30.9 nm) form ragged, densely packed agglomerates, and the largest grains (59.1 nm) are massive spheres with a smooth surface and homogeneous internal texture. Similar, co-occurring ragged and smooth spheres but of different composition were found in both smokes, particularly in S525 (see, Table 2). The present study cannot set sharp boundaries, but it can be generalized that grains smaller than ~35 nm and grains larger than ~100 nm are homogeneous spheres. Grains of intermediate size can be either massive, fuzzy clusters of condensate grains due to variable dust density inside the condensation chamber, or smooth spheres. This textural change as an apparent function of size suggests that the formation of smooth spheres could be related to the surface free energy. A role for surface free energy in condensed smokes was previously demonstrated for stability of the forsterite + SiO_2 assemblage during thermal annealing of a magnesiosilica smoke (Rietmeijer et al. 1986).

Alumina and low-silica aluminosilica grains

Sample S25 contains extremely rare amorphous AlO_x grains that co-occur with amorphous, low-silica aluminosilica grains (Al_2O_3 = 93.9 wt%; range = 92–95 wt%) forming partially fused necklaces. These grains are extremely sensitive to interactions with the incident electron beam that causes instantaneous vesicle formation (Fig. 7). Ferroaluminosilica spheres (>30 nm) with <50 wt% SiO_2 in S525 are also extremely sensitive to interactions with the incident electron beam. They too rapidly develop a vesicular texture (Fig. 8). This extreme instability seems to be related to a high-Al content.

Binary and ternary grain compositions

Condensation of pre-mixed, metal-oxide vapor molecules is a stochastic process that initially yields pure metal-oxide dust. We assume that the smallest amorphous grains are compositionally the closest to the condensed gas molecules and define the aluminosilica and ferrosilica DME compositions. The compositions in S25 and S525 match those observed in previous condensation studies. The smallest condensate grain compositions in S525 and S25 perfectly match those in the Al_2O_3-SiO_2 system and the FeO/Fe_2O_3-SiO_2 pseudo-binary system (Table 3). High-silica ($SiO_2 \approx 97$ wt%, Table 2) ferrosilica smoke grains and spheres (S525) are excluded from Table 3 as silica condensates typically contain small amounts of Fe and Al (Rietmeijer and Karner 1999; Rietmeijer et al. 1999b). In general, condensate grains with the

DME compositions seen in previous condensation experiments (Table 3) are scarce in S525 and absent in S25 as a result of extensive mixing and fusion of these condensate grains. The DME ferrosilica and aluminosilica grains in S25 and S525 are shown in Figure 9 along with the ferrosilica and aluminosilica spheres. The present study is the first report of condensate grains (2–46 nm) and large spheres with a high-Si ferroaluminosilica composition (mostly in S525), and 2–17 nm-sized, high-Al ferroaluminosilica smoke grains (SiO_2 = 56.9; Al_2O_3 = 25.8; FeO = 17.3 wt%; Table 2; Figs. 6a and 9).

Sphere compositions

Spheres with compositions similar to, or intermediate between, the smallest grain compositions (Table 2) occur in S525 and S25 due to fusion of agglomerates of these small grains. The

TABLE 3. The smallest condensate compositions in S525 and S25 (Table 2) compared to the DME grains in ferrosilica and aluminosilica smokes

Ferrosilica smoke			
Rietmeijer et al. (1999a, 1999b)		S525/S25	
Mean (FeO wt%)	Range	Mean (FeO wt%)	Range
13	7–18	12.7/14.5	8–20/8–21
29	15–45	31 (one grain)	–
58	Few grains	Not present	–
87.5	75–90	Not present	–
Aluminosilica smoke			
Rietmeijer and Karner (1999)		S525/S25	
Mean (Al_2O_3 wt%)	Range	Mean (Al_2O_3 wt%)	Mean
6.7	1–15	Not present	–
11.5	6–16	15 (few grains)	–
46.7	22–71	47.1/47.1	25–70/22–71
Not present		93.9	92–95
Not present	100 (one grain)	–	

Note: Statistical t-tests comparing the population means in S25 and S525 to those in the previous studies show that the means are not from different populations.

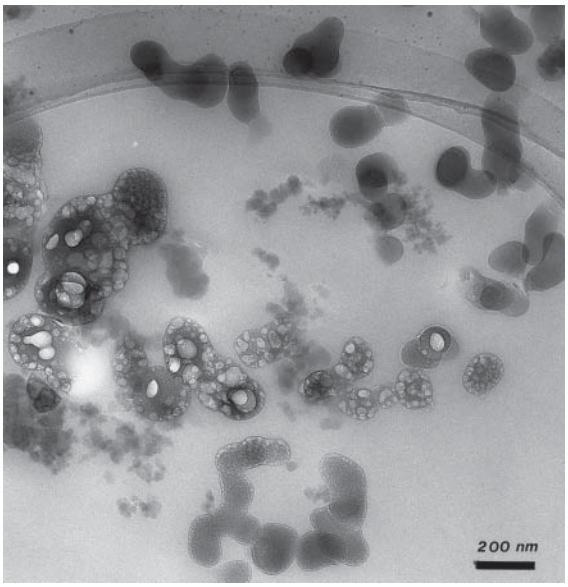

FIGURE 7. TEM image showing smooth, low-silica aluminosilica spheres (top) in S25. When such spheres interacted with the incident electron beam during chemical analysis, they rapidly developed a highly vesicular texture (center). The scale bar is 200 nm.

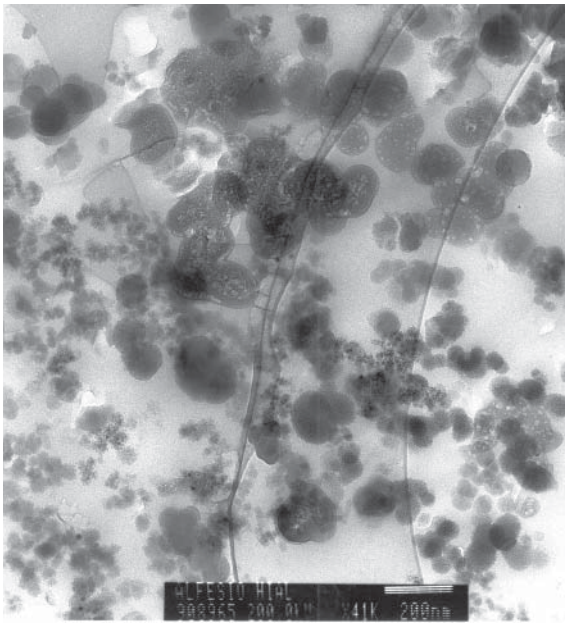

FIGURE 8. TEM image of smooth (bottom) and vesicular (top of the image) ferroaluminosilica spheres due to electron beam interactions in S525. The average sphere composition is SiO_2 = 35.8, Al_2O_3 = 50.5, and FeO = 13.7 wt%. Fine-grained smoke (black/gray) is interspersed among the spheres. The scale bar is 200 nm.

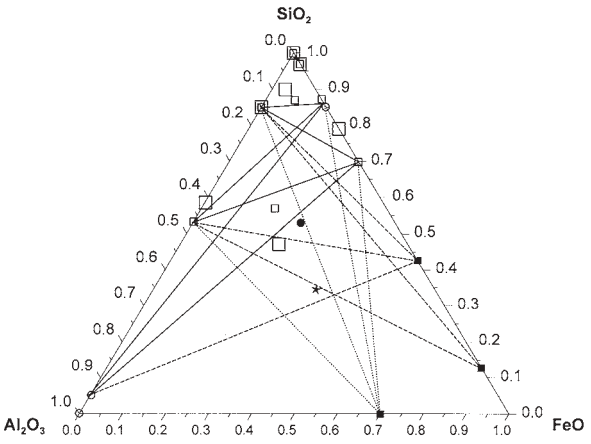

FIGURE 9. Ternary Al_2O_3-FeO-SiO_2 diagram with the compositions of DME condensates in S525 (small open squares) and S25 (small open circles) (Tables 2 and 3) on the Al_2O_3-SiO_2 and FeO-SiO_2 sides; they are connected by solid (mixing) lines. High-Fe ferrosilica DME compositions (from Rietmeijer et al. 1999b) (solid squares) are connected by dashed mixing lines to other DME compositions; dotted mixing lines connect a putative DME Al,Fe-oxide composition (see discussion) to the other DME compositions. Ferroaluminosilica compositions that evolved along any of these mixing lines will be mostly silica-rich ternary grains. Sample S525 contains both small (small open squares) and large (large open squares) spheres with a ferroaluminosilica composition. The latter include a 340 nm size sphere with an Fe-cordierite composition. The black dot represents the largest sphere (450 nm) in S25. The most Fe-rich ferroaluminosilica condensate (star) is defined by two the intersecting (dashed) mixing lines.

t-test of the means of these aluminosilica sphere compositions (Al_2O_3 = means of 47.1 and 41.8 wt%; Table 2) and auto-annealed aluminosilica grains (Al_2O_3 = 41.4 wt%; Rietmeijer and Karner 1999) shows that there is no evidence to suggest that these compositions came from populations having different means. These spheres, and ferrosilica (FeO = 21 wt%) spheres, grew at the expense of the smallest condensate grains, of which only a few remain in the smokes. The ferroaluminosilica sphere size in S525 shows an overall increase along a trend that is more or less sub-parallel to the SiO_2-Al_2O_3 join, with size increasing toward the center of the ternary diagram from 44.2 ± 8.0 nm (range = 29–59 nm) to 103.1 ± 21.1 nm (range = 65–165 nm). Many of these spheres contain an occasionally high density of tridymite grains, 6.0 ± 2.5 nm (range = 2–13 nm) (Fig. 10). These grains were identified by the lattice fringe spacings. They probably formed by solid-state decomposition. The calculated bulk compositions of these spheres, SiO_2 = 55, Al_2O_3 = 31, and FeO = 14 wt%, and those for the ferroaluminosilica smoke grains (Table 2) are not statistically different (t-test), which is an indication that the spheres evolved via isochemical fusion of condensate grain agglomerates.

FeO/Fe_2O_3 in FeSiO grains and hematite identification

The measured saturation magnetization (M_s) for Fe_2O_3 in the ferrosilica sample is 0.36 Am^2/kg (Fig. 11). This value is somewhat smaller than the reference value for hematite (0.5 Am^2/kg) and different from maghémite (65 Am^2/kg; see Dunlop and Özdemir 1997). The measured high remnant coercivity, 110 mT, is more in agreement with hematite. Assuming all paramagnetic iron is Fe^{3+}, a high-field paramagnetic slope of 1.25×10^{-6} m^3/kg of Fe_2O_3 indicates that about 26% of the Fe_2O_3 in the sample is present in paramagnetic form in the ferrosilica phases. This value would be slightly higher for a mixture of Fe^{2+} and Fe^{3+} in these phases. Correcting the M_s from this partitioning of Fe leads to a value of 0.48 Am^2/kg for the Fe-oxide phase, which is in near perfect agreement with the pure hematite value. Assuming that the ferromagnetic grains are pure hematite, the bulk sample should contain 18% hematite. From this assumption, an amount of paramagnetic Fe_2O_3 can be derived independently, viz. 36–18 = 18%, that is, 50% of total Fe_2O_3. This value is higher than the value derived from the paramagnetic slope, suggesting a significant amount of Fe^{2+} in the paramagnetic ferrosilica phase. One could, in principle, compute an Fe^{2+}/Fe^{3+} ratio for the silicates from the present data, but we refrain from doing so, considering the uncertainties in the measurements and the validity of the assumptions. It is likely that the estimate from the M_s measurement, i.e., 18/(18 + 74) = 20% Fe_2O_3 in the silicate phase, is more robust. It is also more in agreement with the Fe amount measured by TEM (see Fig. 4a of Rietmeijer et al. 1999b). The hysteresis parameters, M_{rs}/M_s = 0.18 and H_{cr}/H_c = 14, clearly indicate a mixture of single domain (SD) and superparamagnetic (SP) grains in the sample. The size threshold for the hematite SD/SP ratio is estimated at 25 nm (Dunlop and Özdemir 1997). The average size of the Fe-oxide grains in the sample is 50 nm (Rietmeijer et al. 1999b). A fraction could be polycrystalline grains as the magnetic grain size corresponds to single-crystal grains. We note that some ferrosilica grains contain nanometer precipitates due to post-condensation decomposition (Rietmeijer et al. 1999b).

The ESR response of the sample at room temperature shows a strong line centered at $B_r \approx 325$ mT ($\gamma = 2.06$) and a weak line at $B_r \approx 165$ mT ($\gamma = 4.1$) (Fig. 12). Deviation from the Lorentzian shape of the line at $\gamma = 2.06$ and its large width (circa 900 mT) can be related to the crystal-field symmetry of the Fe ion in the ferrosilica phase. These lines are attributed to Fe^{3+} ions dispersed in a silicate matrix because Fe^{2+} ions have no ESR response (e.g., Calas 1988). The absorption line near $\gamma = 4.3$ is due to isolated Fe^{3+} ions at low-symmetry sites (Balan et al. 1999). The broad signal at $\gamma = 2$ is representative of the total ESR absorption. Similar signals were detected in volcanic glasses (Schlinger et al. 1988; Ananou et al. 2003, 2005) and could be due to small Fe clusters, single-domain particles, or both (Griscom 1984).

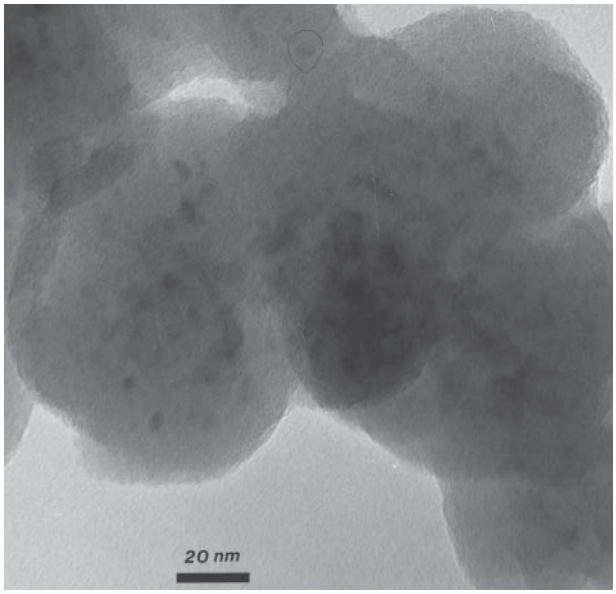

FIGURE 10. TEM image of large ferroaluminosilica spheres in S25 with tridymite grains (dark spots) identified by TEM lattice-fringe imaging. The scale bar is 20 nm.

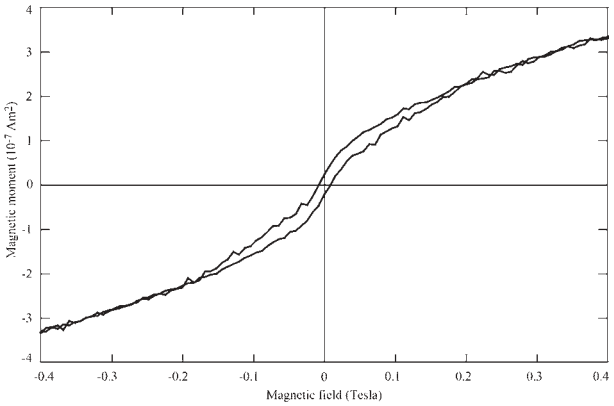

FIGURE 11. Hysteresis loop magnetization as a function of magnetic field, at room temperature, for the vapor-condensed ferrosilica sample, using the Micromag vibrating sample magnetometer in CEREGE. The magnetic field was limited to 0.4 T because of strong increase in the noise level for higher fields.

Although more precise identification of the observed signals would require a temperature-dependent study, the ESR results are in full agreement with those obtained by conventional magnetic methods (Ananou et al. 2005).

In summary, the condensed ferrosilica smoke contains paramagnetic Fe^{3+} ions. These data prove that the two different DME ferrosilica grain compositions previously reported are due to variable Fe^{2+}/Fe^{3+} ratios and that the condensed Fe-oxide grains are overwhelmingly hematite, not maghémite as was originally thought. In considering this result, it is important to note that the FeSiO smoke sample was stored without precaution to avoid possible oxidation with air. With regard to the Fe_2O_3 single crystals, irrespective of the alpha (hematite) or gamma (maghémite) form, originally reported in the smoke, oxidation is not an issue. The original report found two distinct clusters of FeSiO condensate composition that were interpreted to reflect variable FeO/Fe_2O_3 ratios. This interpretation is confirmed by the magnetic measurements. We cannot be absolutely sure that the Fe^{3+}/Fe^{2+} ratio in the stored ferrosilica grains has not increased from their original ratio. Samples S25 and S525 contain few remaining ferrosilica condensate grains after grain mixing and fusion. Their Fe^{3+}/Fe^{2+} ratios will be reflected in the spheres, including the largest spheres with an Fe-cordierite composition.

Discussion

The results for the smokes S525 and S25 show that: (1) the bulk gas-phase composition is clearly not a prime controlling parameter for grain formation and growth; (2) grains include pure alumina and low-silica aluminosilica compositions not seen previously in a condensed Al-SiO-O_2-H_2 vapor (Rietmeijer and Karner 1999); (3) there is a dearth of amorphous, high-Fe ferrosilica grains, unlike condensation in Fe-SiO-H_2-O_2 vapor (Rietmeijer and Nuth 1991; Rietmeijer et al. 1999b); (4) grains are subject to extreme agglomeration and isochemical fusion into large homogeneous ferroaluminosilica spheres; (5) grains show ternary mixing along lines defined by the compositions of DME dust condensates; and (6) grains show evidence for the formation of amorphous spheres with an Fe-cordierite composition. The only concrete conclusion that can be drawn from the infrared spectra of the S25 and S525 smokes (Nuth 1996; Nuth et al. 1988) is that these spectral features are not directly related to the bulk composition of the smokes and that both Fe (Fe^{2+}; Fe^{3+}) and Al probably exist in more than one phase, consistent with the results from the present study.

The Al-oxide, low-silica aluminosilica, and Al-rich ferroaluminosilica condensate smoke grains are extremely unstable. It is well known that corundum (alumina) is a poor glass-forming compound, but in our smokes, these grains condensed unavoidably during the non-equilibrium condensation process. When placed under the incident electron beam, they literally evaporated. To illustrate our point, we show pure alumina grains that condensed in an AlO-O_2-H_2 vapor in the same apparatus as was used for the ferroaluminosilica smokes. They, too, instantly developed the same vesicular texture, when interacting with the incident electron beam (Fig. 13). These observations confirm that extreme instability is a fundamental property of non-equilibrium vapor-phase condensation, at least in materials that are poor glass formers.

An unintended by-product of the vapor-phase condensation experiments was a need to adjust the FeO- and MgO-rich portion of the FeO/Fe_2O_3-SiO_2 and MgO-SiO_2 phase diagrams to accommodate the low-silica ferrosilica and magnesiosilica DME condensates by introducing a new eutectic between a metal-oxide + liquid field and a two-liquid field (cf., Fig. 2) (Rietmeijer et al. 1999b, 2002a). Most silicate phase diagrams are based on quenched-liquid experiments, which have led to two different versions for the Al_2O_3-SiO_2 phase diagram (Aramaki and Roy 1962; Aksay and Pask 1975; Risbud and Pask 1978), depend-

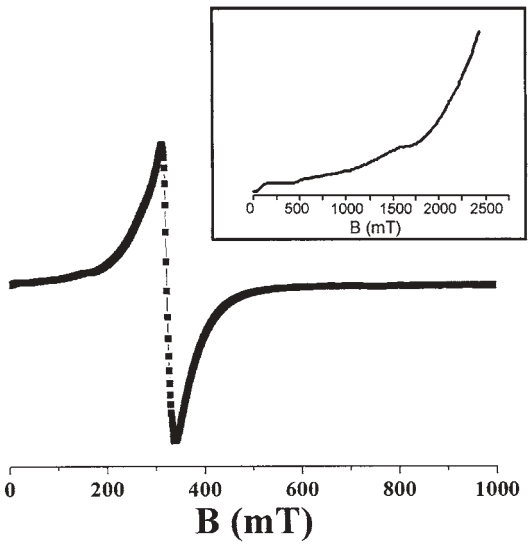

Figure 12. Electron spin resonance spectroscopy signal of the condensed ferrosilica smoke at room temperature. The weak resonance line near $B_r \approx 165$ mT is shown in the insert.

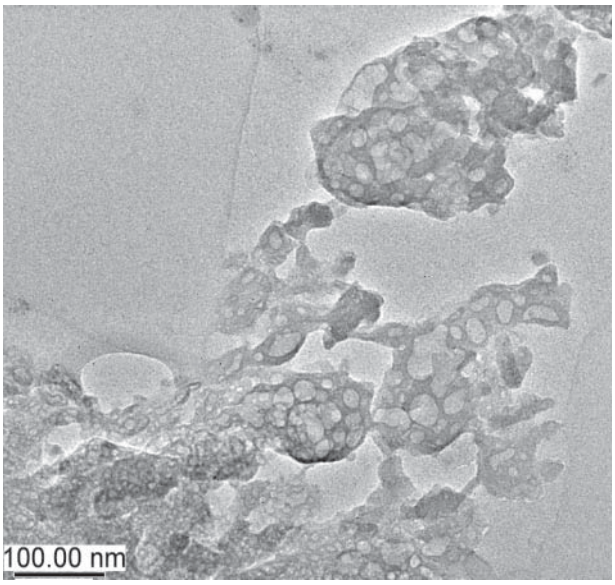

Figure 13. High-resolution TEM micrograph of the vesicular texture produced in condensed pure alumina grains after interaction with the incident electron beam. The scale bar is 100 nm.

ing upon whether mullite melts congruently or not (Klug et al. 1987). The low-silica aluminosilica condensates reported here would support a two-liquid field between the stability fields of mullite + liquid and corundum + liquid. This new liquidus topology would allow DME behavior in the silica-poor part of the Al_2O_3-SiO_2 phase diagram, lending support for mullite stability as Aramaki and Roy (1962) had proposed. We show three DME aluminosilica compositions (Figs. 6 and 9).

S25 and S525 show widespread growth of ferroaluminosilica grains due to complete fusion of smoke grains along mixing lines defined by DME compositions. The mixing efficiency was such that almost all DME ferrosilica grains with a high Fe^{2+} content, including serpentine dehydroxylate grains (solid squares along the FeO-SiO_2 join in Fig. 9), were consumed. The Fe-rich ferroaluminosilica grains (SiO_2 = 34, Al_2O_3 = 28, FeO = 38 wt%; star in Fig. 9) suggest that condensate grains with these DME compositions were present originally. The phase relationships in the Fe-oxide–Al_2O_3 system are controlled by the Fe^{2+}/Fe^{3+} ratio (for a summary, see Eitel 1965), and clearly show that solids with a DME composition cannot be formed in the Fe_2O_3-Al_2O_3 system. However, they could form in the FeO-Al_2O_3 binary system in the high-FeO region between wüstite and hercynite (Fischer 1955; Eitel 1965). Quenched-melt experiments by Fischer (1955) discredited the results from an earlier quenched-melt study on slag systems (Hay et al. 1937) that identified a $3FeO{\cdot}Al_2O_3$ compound coexisting with FeO and hercynite. This, probably metastable, quenched-melt Fe,Al-oxide compound (ca. 70 wt% FeO) defines a DME eutectic ferroalumino composition in our condensation experiments (see Fig. 6). Condensation in an SiO-H_2 (or Ar) vapor typically produces a metastable amorphous Si_2O_3 silicate (Nuth and Donn 1984) that in the condensing Al-Fe-SiO-O_2-H_2 vapors could have promoted the formation of the metastable Fe,Al-oxide compound, viz. (1) $Si_2O_3 + Al_2O_3 = 2SiO_2 + 2AlO$ and (2) $2AlO + Fe_2O_3 \Rightarrow 2FeO{\cdot}Al_2O_3$ (59 wt% FeO). The high-Si, DME ferrosilica compositions (Fig. 9) suggest that variable Fe^{2+}/Fe^{3+} ratios existed during condensation, which is consistent with the magnetic measurements on the ferrosilica smoke. We have no such measurements for the S25 and S525 smokes.

Quenched-melt experiments to determine the equilibrium phase relationships in the system FeO-Al_2O_3-SiO_2 found that "iron cordierite crystallizes with some reluctance" in favor of other metastable phase relationships (Schairer and Yagi 1952). Yet, Fe-cordierite is found in volcanic rocks, thermally metamorphosed iron ore, pyrometamorphic buchite (Schairer and Yagi 1952; Kitamura and Hiroi 1982), and blast-furnace linings (Richardson and Rigby 1949). This natural and anthropogenic Fe-cordierite is metastable (Richardson and Rigby 1949). For a study that was intended to investigate changes in the magnetic properties of magnetite due to flash-heating, three disks of this mineral separated by a layer of aluminosilica glass wool (each ~1 cm thick) were placed inside a cylinder connected by a copper wire to a rocket fired into an overhead cloud at the Langmuir Laboratory for Atmospheric Research (New Mexico). A lightning strike passed through the entire length of the cylinder causing a 1 cm wide hole in the slabs and wool, which showed a brownish discoloration and the presence of micrometer-sized spheres. The spheres have an Fe-cordierite composition from a reaction of aluminosilica glass with magnetite induced by the lightning strike; the cordierite clearly formed under non-equilibrium conditions (Rietmeijer et al. 1999c).

Many chondritic IDPs contain Mg,Fe-bearing aluminosilica grains of unknown origin (Thomas et al. 1989; Rietmeijer 1992, 1998). It is possible that these grains are solar nebula condensates, and it is interesting that vapor-condensation experiments conducted under microgravity conditions could reproduce these particular aluminosilica compositions (Kobatake et al. 2001). Cordierite is present in Ca,Al-rich inclusions in the Allende meteorite (Fuchs 1969) and metastable yagiite, an osumilite-type (Schreyer and Schairer 1962) silicate, was found in an iron meteorite (Bunch and Fuchs 1969). These extraterrestrial silicates are Mg-rich but results from the present study would suggest that they could be metastable phases from non-equilibrium solar nebula condensation.

The formation of solids with DME compositions in vapor-phase condensation experiments might be generalized to include physical conditions of high heating and cooling rates such as might be naturally encountered in meteorite impact craters and their ejecta or during coal combustion of materials meeting the appropriate chemical boundary conditions. Rietmeijer et al. (2000) noted that the unique compositions of aluminosilica coal fly ash spheres indicated a non-equilibrium formation process. Here we note that the compositions of ferroaluminosilica fly ash particles $PM_{2.5}$ and $PM_{2.5+}$ from some eastern U.S. coals (Chen et al. 2004) resemble the distributions reported for sample S525. Such metastable solids would be highly reactive in their depositional environments with potentially hazardous health effects (Chen et al. 2004). Metastable eutectic behavior found in vapor-phase condensation experiments of the type reported here might well have much wider implications.

ACKNOWLEDGMENTS

We thank Paul Withey for preparing the pure alumina condensate. We appreciate reviews by Mike Zolensky and John Bradley, and the editorial efforts by Dave Vaniman to improve our presentation. This work is based upon work supported by the National Aeronautics and Space Administration under grants NAG5-11762 and NNG05GG10G issued through the Office of Space Science and by RTOPS from the Cosmochemistry and Origins of Solar Systems Research Programs (FJMR). J.A.N. is grateful for the support that he has received from the Cosmochemistry Program at NASA Headquarters. A.P. acknowledges a grant from the NASA Goddard Space Flight Center.

REFERENCES CITED

Aasland, S. and McMillan, P.F. (1994) Density-driven liquid-liquid phase separation in the system Al_2O_3-Y_2O_3. Nature, 369, 633–636.

Aksay, I.A. and Pask, J.A. (1975) Stable and metastable equilibria in the system SiO_2-Al_2O_3. Journal American Ceramic Society, 58, 507–512.

Ananou, B., Regnier, S., Ksari, Y., Marfaing, J., Stepanov, A., Touchard, Y., and Rochette, P. (2003) Detection of diluted marine tertiary tephra by ESR and magnetic susceptbility measurements. Geophysical Journal International, 155, 341–349.

Ananou, B., Baronnet, A., Ksari, Y., Marfaing, J., Regnier, S., Rochette, P., Sulpice A., and Stepanov, A. (2005) Magnetic properties of marine tertiary tephra investigated over a wide temperature. Journal Magnetism and Magnetic Materials, 293, 816–825.

Anders, E. and Grevesse, N. (1989) Abundances of the elements: Meteoritic and solar. Geochimica et Cosmochimica Acta, 53, 197–214.

Aramaki, S. and Roy, R. (1962) Revised equilibrium diagram for the system Al_2O_3-SiO_2. Journal American Ceramic Society, 45, 229–242.

Balan, E., Allard, T., Bouzot, B., Morin, G., and Muller, J.P. (1999) Structural Fe^{+3} in natural kaolinites: New insights from ESR spectra fitting and at X and Q-Band frequencies. Clays and Clay Minerals, 47, 605–616.

Baronnet, A. (1984) Growth kinetics of the silicates. A review of basic concepts. Fortschritte der Mineralogie, 62, 187–232.

Bouwman, J., Meeus, G., de Koter, A., Hony, S., Dominik, C., and Waters, L.B.F.M.

(2001) Processing of silicate dust grains in Herbig Ae/Be systems. Astronomy and Astrophysics, 375, 950–962.
Bradley, J.P. (1994) Chemically anomalous, pre-accretionally irradiated grains in interplanetary dust from comets. Science, 265, 925–929.
Bradley, J.P., Keller, L.P., Snow, T., Hanner, M.S., Flynn, G.J., Gezo, J.C., Clemett, S.J., Brownlee, D.E., and Bowey, J.E. (1999) An infrared spectral match between GEMS and interstellar grains. Science, 285, 1716–1718.
Bunch, T.E. and Fuchs, L.H. (1969) Yagiite, a new sodium-magnesium analogue of osumilite. American Mineralogist, 54, 14–18.
Calas, G. (1988) Electron paramagnetic resonance. In F.C. Hawthorne, Ed., Spectroscopic Methods in Mineralogy and Geology, 18, p. 513–571. Reviews in Mineralogy, Mineralogical Society of America, Chantilly, Virginia.
Chen, Y., Shah, N., Huggins, F.E., Huffman, G.P., Linak, W.P., and Miller, C.A. (2004) Investigation of primary fine particulate matter from coal combustion by computer-controlled scanning electron microscopy. Fuel Processing. Technology, 58, 743–761.
De, B.R. (1979) Disequilibrium condensation environments in space: A frontier in thermodynamics. Astrophysics and Space Science, 65, 191–198.
Donn, B. and Nuth, J.A. (1985) Does nucleation theory apply to the formation of refractory circumstellar grains? Astrophysical Journal, 288, 187–190.
Dunlop, D. and Özdemir, Ö. (1997) Rock Magnetism: Fundamentals and Frontiers, 573 p. Cambridge University Press, New York.
Ehlers, E.G. (1972) The Interpretation of Geological Phase Diagrams, 280 p. W.H. Freeman, San Francisco, California.
Eitel, W. (1965) Silicate Science, Vol. II, Dry silicate systems, 553 p. Academic Press Inc., New York.
Fischer, W.A. (1955) EMF-Messungen in den Systemen FeO-Al_2O_3 und MgO-Al_2O_3 sowie Beobachtungen über die Diffusion von FeO in Al_2O_3 bei 1500 °C. Silicates Industriels, 20, 244–254 (in German).
Fuchs, L.H. (1969) Occurrence of cordierite and aluminous orthoenstatite in the Allende meteorite. American Mineralogist, 54, 1645–1653.
Griscom, D.L. (1984) Ferromagnetic resonance of precipitated phases in natural glasses. Journal of Non-Crystalline Solids, 67, 81–118.
Grossman, L. and Larimer, J.W. (1974) Early chemical history of the solar system. Reviews Geophysics and Space Physics, 1, 71–101.
Hay, R., McIntosh, A.B., Rait, J.R., and White, J. (1937) Slag Systems. Journal of the East of Scotland Iron and Steel Institute, 44, session 1936/1937, 85–92.
Highmore, R.J. and Greer, A.L. (1989) Eutectics and the formation of amorphous alloys. Nature, 339, 363–365.
Keller, L.P., Messenger, S., and Bradley, J.P. (2000) Analysis of a deuterium-rich interplanetary dust particle and implications for presolar materials in IDPs. Journal Geophysical Research and Space Physics, 105, 10397–10402.
Kitamura, M. and Hiroi, Y. (1982) Indialite from Unazuki pelitic schist, Japan, and its transition texture to cordierite. Contribution to Mineralogy and Petrology, 80, 110–116.
Klug, F.J., Prochazka, S., and Doremus, R.H. (1987) Alumina-silica phase diagram in the mullite region. Journal American Ceramic Society, 70, 750–759.
Kobatake, H., Tsukamoto, K., Yokoyama, E., Satoh, H., and Yurimoto, H. (2001) In situ Investigation for the origin of interplanetary dust particles under microgravity. Lunar and Planetary Science, 32, abstract 1550, Lunar and Planetary Institute, Houston, Texas (CD-rom).
Larimer, J.W. (1967) Chemical fractionations in meteorites-I. Condensation of the elements. Geochimica et Cosmochimica Acta, 31, 1215–1238.
——— (1988) 7.1. The cosmochemical classification of the elements. In J.F. Kerridge and M.S. Matthews, Eds., Meteorites and the Early Solar System, p. 375–389. University of Arizona Press, Tucson.
Lord, H.C., III (1965) Molecular equilibria and condensation in a solar nebula and cool stellar atmospheres. Icarus, 4, 279–288.
MacKenzie, K.J.D. and Meinhold, R.H (1994) Thermal reactions of chrysotile revisited: A ^{29}Si and ^{25}Mg MAS NMR study. American Mineralogist, 79, 43–50.
Messenger, S. (2000) Identification of molecular-cloud material in interplanetary dust particles. Nature, 404, 968–971.
Molster, F.J. and Waters, L.B.F.M. (2003) The mineralogy of interstellar and circumstellar dust. In T.K. Henning, Ed., Astromineralogy, Lecture Notes Physics, 609, p. 121–170. Springer, Heidelberg, Germany.
Nelson, R., Thiemens, M., Nuth, J., and Donn, B. (1989) Oxygen isotopic fractionation in the condensation of refractory smokes. In G. Ryder and V.L. Sharpton, Eds., Proceedings of the 19th Lunar and Planetary Science Conference, p. 559–563, Cambridge University Press and Lunar and Planetary Institute, Cambridge and Houston, Texas.
Nuth, J.A. (1996) Grain formation and metamorphism. In J.M. Greenberg, Ed., The Cosmic Dust Connection, p. 205–221. Kluwer Academic Publishers, the Netherlands.
Nuth, J.A. and Donn, B. (1984) Thermal metamorphism of Si_2O_3 (a circumstellar dust analog). Proceedings Lunar and Planetary Science Conference 14, part 2, Journal Geophysical Research, 89, Supplement, B657–B661.
Nuth, J.A., Nelson, R.N., Moore, M., and Donn, B. (1988) Experimental studies of circumstellar, interstellar and interplanetary refractory grains analogs. In E. Bussoletti C. Fusco, and G. Longo, Eds., Experiments on Cosmic Dust Analogues, p. 191–207. Kluwer Academic Publishers, the Netherlands.
Nuth, J.A, Hallenbeck, S.L., and Rietmeijer, F.J.M. (2000) Laboratory studies of silicate smokes: Analog studies of circumstellar materials. Journal Geophysical Research, 105(A5), 10387–10396.
Nuth, J.A., Rietmeijer, F.J.M., and Hill, H.G.M. (2002) Condensation processes in astrophysical environments: The composition and structure of cometary grains. Meteoritics and Planetary Science, 37, 1579–1590.
Papike, J.J., Ed. (1998) Planetary Materials, 36, 1052 p. Reviews in Mineralogy, Mineralogical Society of America, Chantilly, Virginia.
Petaev, M.I. and Wood, J.A. (1998) The condensation with partial isolation (CWPI) model of condensation in the solar nebula. Meteoritics and Planetary Science, 33, 1123–1137.
Prigogine, I. (1978) Time, structure, and fluctuations. Science, 201, 777–785.
——— (1979) Irreversibility and randomness. Astrophysics and Space Science, 65, 371–381.
Richardson, H.M. and Rigby, G.R. (1949) The occurrence of iron-cordierite in blast-furnace linings. Mineralogical Magazine, 30, 547–556.
Rietmeijer, F.J.M. (1992) Mineralogy of primitive chondritic protoplanets in the early solar system. Trends in Mineralogy, 1, 23–41, Council Scientific Research Integration, India.
——— (1998) Interplanetary Dust Particles. In J.J. Papike, Ed., Planetary Materials, 36, 2-1–2-95. Reviews in Mineralogy, Mineralogical Society of America, Chantilly, Virginia.
——— (1999) Metastable non-stoichiometric diopside and Mg-Wollastonite: An occurrence in an interplanetary dust particle. American Mineralogist, 84, 1883–1894.
——— (2002) The earliest chemical dust evolution in the solar nebula. Chemie der Erde, 62, 1–45.
Rietmeijer, F.J.M. and Karner, J.M. (1999) Metastable eutectics in the Al_2O_3-SiO_2 system explored by vapor phase condensation. Journal of Chemical Physics, 110, 4554–4558.
Rietmeijer, F.J.M. and Nuth, J.A. (1991) Tridymite and maghémite formation in a Fe-SiO smoke. In G. Ryder and V.L. Sharpton, Eds., Proceedings Lunar Planetary Science Conference, 21, 591–599. Lunar and Planetary Institute, Houston, Texas.
——— (2005) Laboratory simulation of Mg-rich ferromagnesiosilica dust: The first building blocks of comet dust. Advances in Space Research, In press/on-line, DOI:10.1016/j.asr.2005.03.113.
Rietmeijer, F.J.M., Nuth, J.A., and Mackinnon, I.D.R. (1986) Analytical electron microscopy of Mg-SiO smokes: Comparison with XRD and Infrared studies. Icarus, 65, 211–222.
Rietmeijer, F.J.M., Nuth, J.A., III, and Karner, J.M. (1999a) Metastable eutectic condensation in a Mg-Fe-SiO-H_2-O_2 vapor: Analogs to circumstellar dust. Astrophysical Journal, 527, 395–404.
——— (1999b) Metastable eutectic gas to solid condensation in the FeO-Fe_2O_3-SiO_2 system. Physical Chemistry Chemical Physics, 1, 1511–1516.
Rietmeijer, F.J.M., Karner, J.M., Nuth, J.A., III, and Wasilewski, P.J. (1999c) Nanoscale phase equilibrium in a triggered lightning strike experiment. European Journal Mineralogy, 11, 181–186.
Rietmeijer, F.J.M., Nuth, J.A., III, Jablonska, M., and Karner, J.M. (2000) Metastable eutectic Equilibrium in Natural Environments: Recent Developments and Research Opportunities. Trends in Geochemistry, 1, 29–51, Research Trends, Trivandrum, India.
Rietmeijer, F.J.M., Nuth, J.A., III, Karner, J.M., and Hallenbeck, S.L. (2002a) Gas to solid condensation in a Mg-SiO-H_2-O_2 vapor: Metastable eutectics in the MgO-SiO_2 phase diagram. Physical Chemistry Chemical Physics, 4, 546–551.
Rietmeijer, F.J.M., Hallenbeck, S.L., Nuth, J.A., III, and Karner, J.M. (2002b) Amorphous magnesiosilicate smokes annealed in vacuum: The evolution of magnesium silicates in circumstellar and cometary dust. Icarus, 156, 269–286.
Rietmeijer, F.J.M., Nuth, J.A., III, and Nelson, R.N. (2004) Laboratory hydration of condensed magnesiosilica smokes with implications for hydrated silicates in IDPs and comets. Meteoritics and Planetary Science, 39, 723–746.
Risbud, S.H. and Pask, J.A. (1978) SiO_2-Al_2O_3 Metastable phase equilibrium diagram without mullite. Journal of Materials Science, 13, 1449–1454.
Schairer, J.F. and Yagi, K. (1952) The system FeO-Al_2O_3-SiO_2. American Journal of Science, Bowen Volume, 471–512.
Schlinger, C.M., Griscom, D., Papaefthymiou, G.C., and Veblen, D.R. (1988) The nature of magnetic single domains in volcanic glasses of the KBS Tuff. Journal of Geophysical Research, 93, 9137–9155.
Schreyer, W. and Schairer, J.F. (1962) Metastable osumilite- and petalite-type phases in the system MgO-Al_2O_3-SiO_2. American Mineralogist, 47, 90–104.
Thomas, K.L., Klöck, W., and McKay, D.S. (1989) Compositional comparison of IDP glasses and UOC chondrule glasses (abstract). Meteoritics, 24, 332.
Wark, D.A. (1979) Birth of the presolar nebula: The sequence of condensation revealed in the Allende meteorite. Astrophysics Space Science, 65, 275–295.
Wood, J.A. and Hashimoto, A. (1993) Mineral equilibrium in fractionated nebular systems. Geochimica et Cosmochimica Acta, 57, 2377–2388.

Manuscript received September 23, 2005
Manuscript accepted March 25, 2006
Manuscript handled by David Vaniman